***JKPK (JURNAL KIMIA DAN PENDIDIKAN KIMIA)**, Vol. 10, No. 3, 2025* *pp. 445-461*
Chemistry Education Study Program, Universitas Sebelas Maret *ISSN 2503-4146*
https://jurnal.uns.ac.id/jkpk *ISSN 2503-4154 (online)*

Molecular Dynamics Simulation Study: Mechanism of Cationic and Anionic Dyes Adsorption on Montmorillonite

Febriati Dian Mubarokah[1*], Mia Ledyastuti[2], Muhammad Ali Zulfikar [2]

[1]Department of Chemistry Education, Faculty of Science and Mathematics Education, Universitas Pendidikan Indonesia, Bandung, Indonesia
[2]Department of Chemistry, Faculty of Science and Mathematics, Institut Teknologi Bandung, Bandung, Indonesia

ABSTRACT

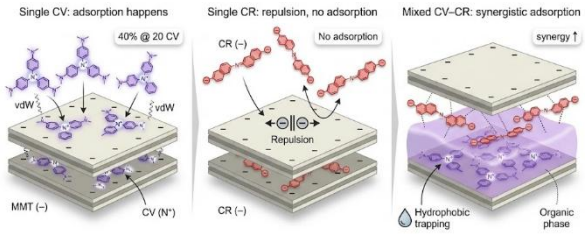

Discharging dye-containing wastewater can severely degrade water quality. Adsorption is widely studied because it is selective, effective, and relatively low-cost. This work examines the adsorption of a cationic dye, crystal violet (CV), and an anionic dye, congo red (CR), on montmorillonite clay (MMT) using molecular dynamics simulations in GROMACS. Molecular topologies were built with a combined ClayFF and CHARMM36 force field. Simulations used a 6 nm × 6 nm × 6 nm box filled with SPC/E water (spce.gro). After minimization and NVT and NPT equilibration, production runs were conducted for 50 ns (25,000,000 steps) with a time step of 2 fs at 300 K and 1 bar. Single-dye and mixed-dye systems were compared to clarify adsorption mechanisms. In the single CV system, the best performance was observed at 20 CV molecules, resulting in 40% adsorption. Radial distribution analysis indicates that adsorption is dominated by van der Waals interactions between the negatively charged MMT surface and the quaternary ammonium site of the CV ($-N^+$). In contrast, CR was not adsorbed in the single CR system because electrostatic repulsion prevents approach to the negatively charged clay. In mixed CV–CR systems, adsorption of both dyes increased, revealing synergistic behavior. CV enters the MMT interlayer and forms an organic phase, which then immobilizes CR through hydrophobic interactions, allowing CR adsorption despite its unfavorable electrostatic interactions under realistic wastewater conditions.

Keywords: *Adsorption; Montmorillonite; Dyes; Molecular Dynamics; GROMACS..*
**Corresponding Author: febriatidian@upi.edu*
How to cite: F.D. Mubarokah, M. Ledyastuti, and M.A. Zulfikar, "Molecular Dynamics Simulation Study: Mechanism of Cationic and Anionic Dyes Adsorption on Montmorillonite," *Jurnal Kimia dan Pendidikan Kimia (JKPK)*, vol. 10, no. 3, pp.445-461, 2025. [Online]. Available: 10.20961/jkpk.v10i3.100095
Received: *2025-03-04* ***Accepted:*** *2025-07-29* ***Published:*** *2025-12-31*

INTRODUCTION

One of Indonesia's manufacturing sectors that has been strengthened to enter the Industry 4.0 era is the textile industry [1], [2]. However, the growth of the textile and apparel industry has not been accompanied by adequate wastewater management [3], [4]. According to the World Bank, 17–20% of industrial water pollution originates from textile effluents [5]. This is largely due to the extensive use of dyes in the industry, with more than 10,000 dye types in commercial use and over 7 × 10^5 tons of synthetic dyes produced annually [6]. The presence of dyes in wastewater can cause severe water pollution because many dyes are toxic and potentially carcinogenic. In addition, dyes often exhibit high resistance to light exposure, pH variation, and microbial degradation, which makes them persistent in the environment. For example, the half-life of the hydrolyzed dye Reactive Blue 19 is

approximately 46 years at pH 7 and 25 °C [7], [8]. Therefore, discharging dye-containing wastewater without prior treatment can degrade water quality and pose a threat to both aquatic ecosystems and human health [9].

The adverse impacts of textile wastewater on water quality have encouraged extensive research on treatment methods to ensure that effluents can be discharged without causing environmental harm. In recent years, various techniques have been proposed for treating dye-containing wastewater, including biodegradation [10], electrocoagulation [11], membrane filtration [12], ion exchange resins [13], coagulation flocculation [14], photocatalysis [15], and adsorption [16], [17]. However, each method has limitations. Toxic dyes can inhibit biodegradation, while coagulation-based methods often generate large volumes of sludge. Other concerns include a short operational lifetime, high costs, the need for specialized equipment, high energy consumption, slow kinetics, and the potential formation of harmful byproducts [16]. Among these options, adsorption is widely regarded as a promising approach because of its selectivity, relatively low operating cost, simplicity, high removal efficiency, and the possibility of adsorbent regeneration and reuse [18]. These advantages make adsorption particularly suitable for the textile industry, which requires wastewater treatment methods that are both effective and economically feasible.

In recent years, numerous adsorbents have been investigated for dye removal, with clay-based materials being among the most widely studied. Clay is abundant, nontoxic, and inexpensive, and it can exhibit considerable adsorption capacity. One clay mineral that has attracted significant attention in wastewater treatment is montmorillonite [19]. Montmorillonite (MMT) carries a permanent negative charge resulting from isomorphic substitution, specifically Al^{3+} replacing Si^{4+} in the tetrahedral layer and Mg^{2+} replacing Al^{3+} in the octahedral layer. This negative charge is balanced by exchangeable interlayer cations (for example, Na^{+} and Ca^{2+}), which enables MMT to adsorb cationic contaminants effectively through ion exchange [20].

Adsorption has been widely explored for treating water contaminated with dyes such as crystal violet and congo red [21], [22], [23], [24], [25]. However, most studies have focused on systems containing only a single dye. In industrial-scale textile wastewater, pollutants are rarely limited to one dye type, and effluents commonly contain mixtures of cationic, anionic, and nonionic dyes [26]. Literature discussing the simultaneous adsorption of cationic and anionic dyes on adsorbents remains limited [19], [27], [28]. Therefore, this study further investigates the adsorption mechanisms of mixed cationic and anionic dyes on montmorillonite using a molecular dynamics (MD) simulation approach. MD simulations enable the investigation of structural properties at the molecular level, helping to clarify the relationships between microscopic interactions and macroscopic system behavior. In addition, MD can provide dynamic and thermodynamic information relevant to adsorption processes and support

the interpretation and validation of experimental findings [29], [30], [31].

The dyes examined in this study are Congo red (CR), an anionic dye, and crystal violet (CV), a cationic dye. Congo red contains an azo group (RN═NR) and aromatic rings. It has a complex molecular structure, is toxic, highly soluble in water, and can persist in the environment after discharge, which makes it difficult to degrade. Congo red has also been reported to exhibit carcinogenic effects in humans, and it has therefore been banned in many countries [32], [33]. Crystal violet (CV), in contrast, is a cationic dye that is not readily degraded under natural conditions and is toxic, genotoxic, and carcinogenic. In aquatic environments, CV contamination can induce tumor formation and reproductive disorders in fish. In humans, exposure to CV may cause eye irritation and, in severe cases, respiratory problems, kidney failure, chemical cystitis, permanent blindness, and cancer [34].

In this study, molecular dynamics simulations were performed using the GROMACS package [35]. The adsorption orientations and mechanisms of CV and CR on MMT were investigated in both single-dye systems and mixed-dye systems. The findings are expected to provide molecular-level insights that support future experimental validation and guide potential industrial applications.

METHODS

The molecular structures of crystal violet (CV) and Congo red (CR) were obtained from the PubChem database. The corresponding topology files, including nonbonded parameters (atom types and partial charges) and bonded parameters (bonds, angles, and dihedrals), were generated using the CHARMM GUI server [36]. The force field employed in this system combined ClayFF and CHARMM36 [37] [38]. ClayFF was used to define the interaction parameters for atoms in montmorillonite (MMT), while CHARMM36 was applied to CV and CR.

CV and CR molecules were introduced into the simulation box using the gmx insert-molecules command. The numbers of CV and CR molecules were varied to examine how the adsorption behavior changes with increasing dye concentration. In the single dye systems, 5, 10, 15, and 20 molecules of either CV or CR were added. In the mixed dye systems, the total number of dye molecules and the CV: CR ratio were systematically varied. For a total of 20 molecules, the CV: CR ratios were 1:1, 3:1, 3:2, and 4:1. For a total of 30 molecules, the CV: CR ratios were 1:1, 2:1, 3:2, and 4:1. For a total of 40 molecules, the CV: CR ratios were 1:1, 3:1, 3:2, and 4:1.

The fully constructed system was then solvated with water molecules. The SPC E water model (spc.gro), available in GROMACS, was used in this study. Solvation was performed using the *gmx solvate command*. Depending on the number of dye molecules added, the system contained approximately 5,000 to 6,000 water molecules, as generated automatically during solvation. After solvation, Na^+ or Cl^- ions were introduced using the *gmx genion command* to neutralize the system.

Energy minimization was prepared using the *gmx grompp command*. In this study, the steepest descent algorithm was applied to minimize the system. The equations of motion were integrated using the Verlet algorithm. All bond lengths were constrained using the LINCS method. The van der Waals cutoff distance was set to 1.0 nm, and long-range electrostatic interactions were treated using the Particle Mesh Ewald (PME) method [39].

System equilibration was performed in two stages using the canonical (NVT) and isothermal isobaric (NPT) ensembles. The NVT equilibration was conducted to stabilize the system temperature. A Nose Hoover thermostat was applied for temperature control [40], and the initial temperature was set to 300 K. The NVT run was performed for 100 ps, corresponding to 50,000 steps. Subsequently, NPT equilibration was performed to stabilize the system's pressure and density under conditions representative of the experiments. Pressure was controlled using a Parrinello-Rahman barostat with a target pressure of 1 bar. The NPT equilibration was run for 1 ns, corresponding to 500,000 steps [41].

The production molecular dynamics simulation was then performed for 50 ns (25,000,000 steps) using a two fs time step at 300 K and 1 bar. Temperature and pressure were maintained using the Nose-Hoover thermostat and the Parrinello-Rahman barostat, respectively. The van der Waals cutoff was set to 1.0 nm, while long-range electrostatic interactions were treated using the Particle Mesh Ewald (PME) method.

In this study, the adsorption orientation mechanisms of CV and CR on MMT in both single-dye and mixed-dye systems were analyzed using simulation outputs, including the radial distribution function (RDF), dye mobility via mean square displacement (MSD), and the number of hydrogen bonds formed within the system.

RESULT AND DISCUSSION

1. Crystal Violet Adsorption

Varying the number of CV molecules added to the system was intended to evaluate the adsorption capacity of MMT as the CV concentration increased. In this study, 5, 10, 15, and 20 CV molecules were introduced. A snapshot of the final configuration for the system containing 20 CV molecules is shown in Figure 1.

At the start of the simulation, CV molecules were dispersed in the aqueous phase. After 50 ns of simulation, CV molecules began to aggregate, and some of these aggregates subsequently interacted with the MMT surface. Using the MDAnalysis protocol, the number of CV molecules located within 1 nm of the MMT surface was quantified. As shown in Table 1, increasing the number of CV molecules led to an increase in the number of CV molecules interacting with MMT. This trend is expected because a higher number of CV molecules increases the probability of contact with the MMT surface.

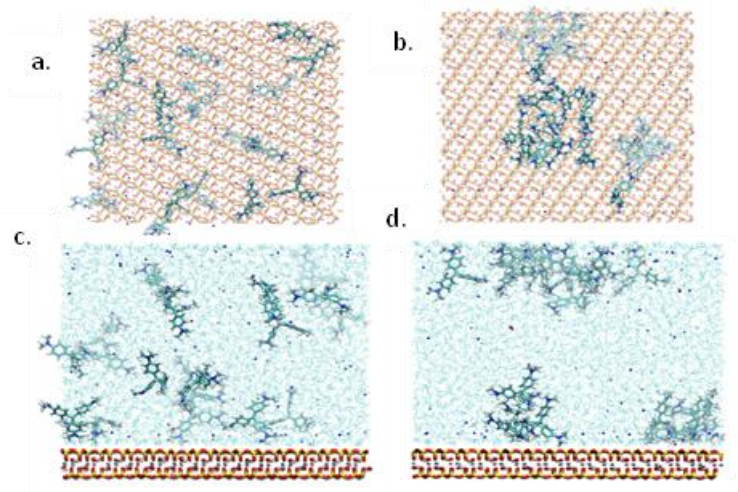

Figure 1. Snapshot of the final results of the 20 CV simulation: a. top view before the simulation; b. top view after the simulation; c. front view before the simulation; d. front view after the simulation

Table 1. Results of MDAnalysis of CV-MMT system simulation

Production Time (ns)	Initial Number of CV	Number of CV adsorbed (VdW)
50	5	3
50	10	3
50	15	5
50	20	8

The trajectory files obtained at the end of the simulations were used to analyze the orientation of CV functional groups and to identify the dominant interactions with MMT. This analysis was performed using the radial distribution function (RDF). The CV structure was divided into several functional groups, as shown in Figure 2. In this study, the reference atom was the surface oxygen at the active sites of MMT. Figure 3 presents the RDF profiles between selected CV functional groups and the MMT surface oxygen atoms. A prominent peak appears at a distance of approximately 0.5 nm, indicating that the dominant interaction between CV and the MMT surface is governed mainly by van der Waals forces [42]

This interpretation is supported by the hydrogen bond analysis shown in Figure 4, which compares the hydrogen bonds formed between CV and MMT with those formed between CV and water. The number of hydrogen bonds between CV and MMT is very low and becomes negligible by the end of the simulation. Hydrogen bonding occurs predominantly between CV and water, and the number of these hydrogen bonds decreases as the simulation proceeds. This trend suggests that CV molecules are adsorbed onto the MMT surface and increasingly form aggregates with other CV molecules, which reduces their interaction with surrounding water molecules. Figure 3 also shows that the highest RDF peak corresponds to the N^+ site in CV. This is

consistent with the negatively charged nature of MMT, which promotes stronger attraction toward the positively charged N^+ center. According to the RDF results (Figure 3), the dominant interaction between the quaternary ammonium (N^+) group of CV and the MMT surface is primarily van der Waals in character [43]. Consistent with previous experimental findings, interactions involving the quaternary amine group are considered the key contribution driving CV adsorption onto the MMT surface [44].

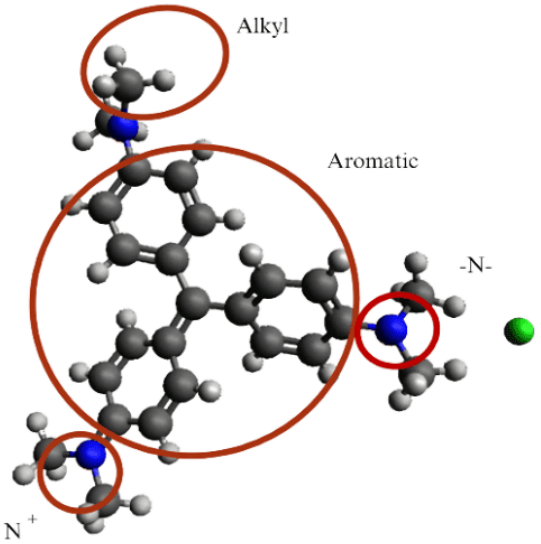

Figure 2. Classification functional group of CV (grey = C, white = H, blue = N, green = Cl).

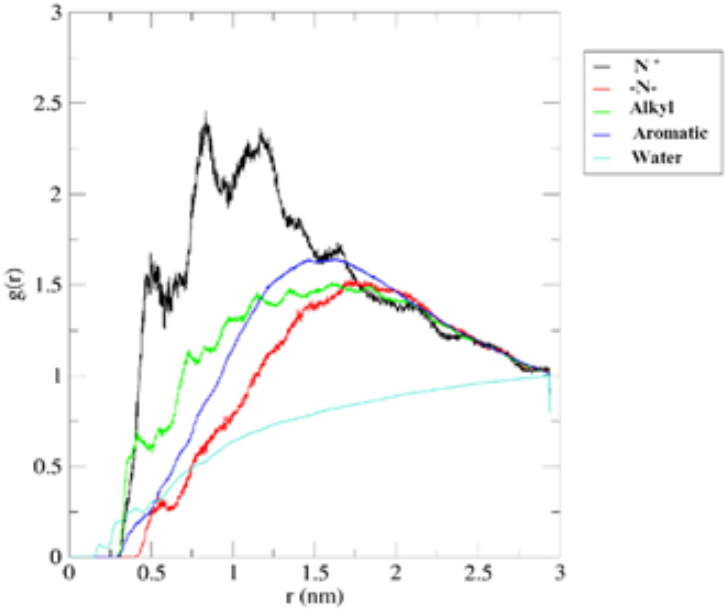

Figure 3. RDF between the functional group of CV and the oxygen atom on the MMT surface

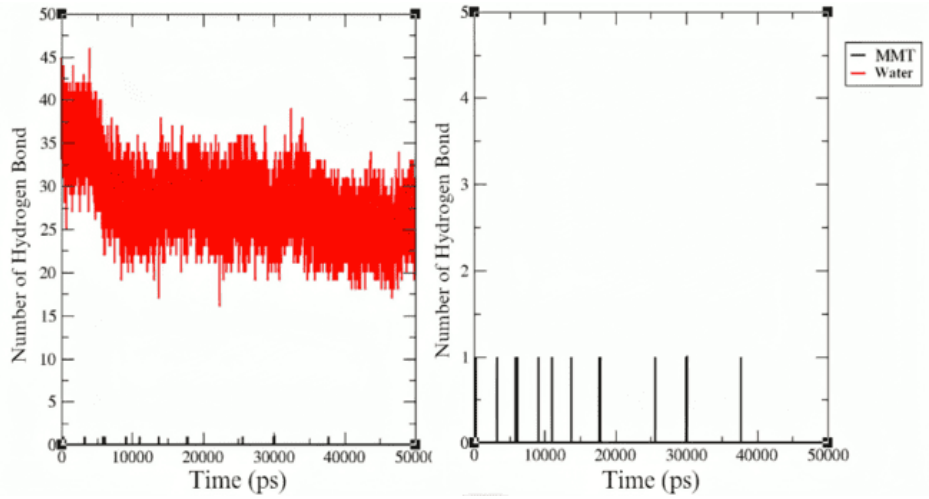

Figure 4. The number of hydrogen bonds in the system, a. CV-water and CV-MMT; b. enlargement of CV-MMT

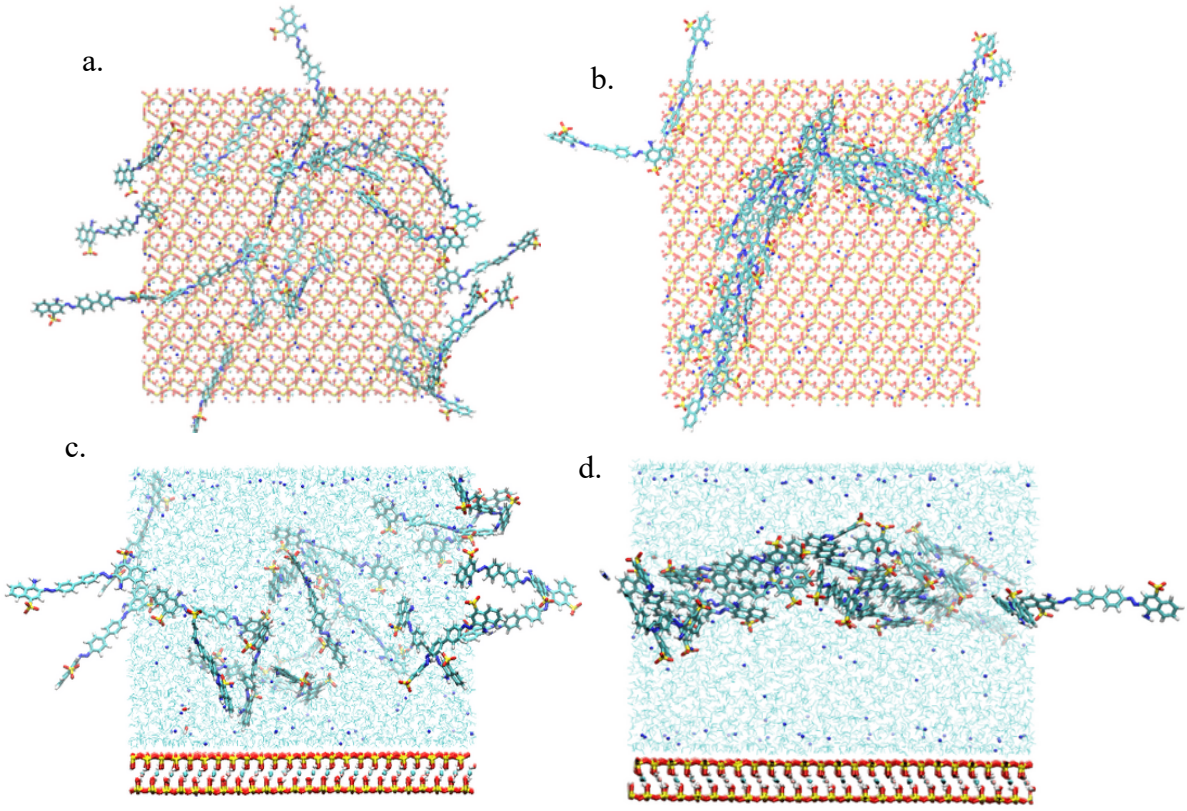

Figure 5. Snapshot of the final results of the 20 CR simulation: a. top view before the simulation; b. top view after the simulation; c. front view before the simulation; d. front view after the simulation

2. Congo Red Adsorption

Figure 5 illustrates the final configuration of the system, which includes CR. Before the simulation, CR molecules were dispersed in the aqueous phase. After 50 ns, CR molecules began to aggregate with each other; however, no adsorption onto the MMT surface was observed. This behavior is also supported by the MDAnalysis results. As shown in Table 2, increasing the number of CR molecules did not increase the number of CR molecules located within the interaction distance from MMT. This indicates that CR did not adsorb onto MMT under the conditions investigated.

.

Table 2. Results of MDAnalysis of the CR-MMT system simulation

Produksi Time (ns)	Initial Number of CR	Number of CR adsorbed (VdW)
50	5	-
50	10	-
50	15	-
50	20	-

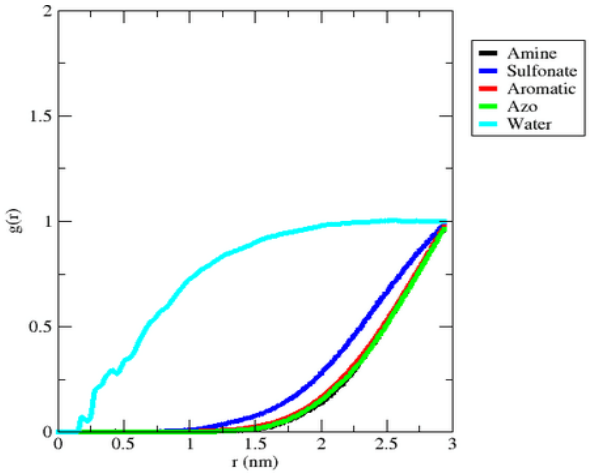

Figure 6. RDF between functional group of CR and oxygen atom on MMT surface.

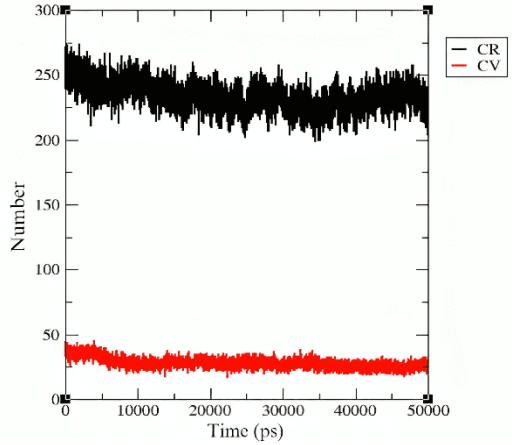

Figure 7. The number of hydrogen bonds in the system, CV-MMT and CR-MMT.

CR has a markedly different structure from CV. CR is an anionic dye, and each molecule carries two negative charges. In principle, CR is less likely to interact with the MMT surface because MMT is also negatively charged. Electrostatic repulsion between CR and the MMT surface, therefore, contributes to the low adsorption capacity of pristine MMT toward CR. For this reason, in experimental studies, MMT is often surface-modified when it is intended for the adsorption of CR or other anionic dyes, to enhance its adsorption performance [32].

Figure 6 presents the RDF profiles, which describe the orientation of CR functional groups (Figure 7) relative to the MMT surface. No pronounced peaks are observed for any CR functional group, indicating that CR has no dominant interaction with MMT. Instead, the water MMT interaction is more prominent than the CR MMT interaction. The RDF peak for water relative to MMT, which appears at approximately 0.25 nm, suggests the formation of hydrogen bonds between water molecules and the MMT surface [45]. This supports the hydrophilic nature of MMT and its strong affinity for water [46].

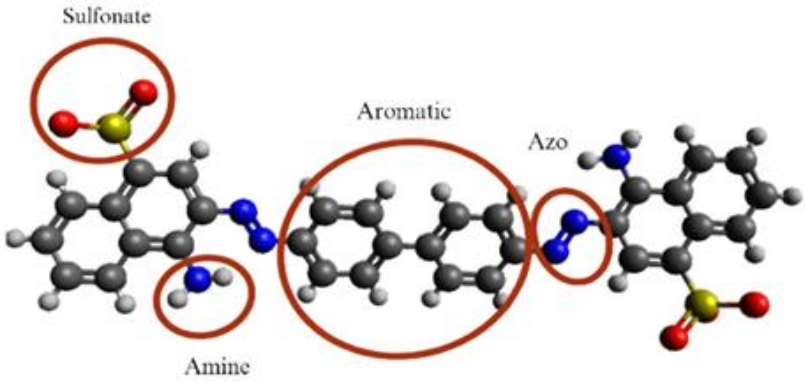

Figure 8. Classification functional group of CR (Grey = C, white = H, blue = N, yellow = S, red = O).

CR has a markedly different structure from CV. CR is an anionic dye, and each molecule carries two negative charges. In principle, CR is less likely to interact with the MMT surface because MMT is also negatively charged. Electrostatic repulsion between CR and the MMT surface, therefore, contributes to the low adsorption capacity of pristine MMT toward CR. For this reason, in experimental studies, MMT is often surface-modified when it is intended for the adsorption of CR or other anionic dyes, to enhance its adsorption performance [32].

Figure 6 presents the RDF profiles, which describe the orientation of CR functional groups (Figure 7) relative to the MMT surface. No pronounced peaks are observed for any CR functional group, indicating that CR has no dominant interaction with MMT. Instead, the water MMT interaction is more prominent than the CR MMT interaction. The RDF peak for water relative to MMT, which appears at approximately 0.25 nm, suggests the formation of hydrogen bonds between water molecules and the MMT surface [45]. This

supports the hydrophilic nature of MMT and its strong affinity for water [46].

Consistently, the hydrogen bond analysis in Figure 8 shows that hydrogen bonding between CR and water is more dominant than that between CV and water. This indicates that CR interacts more strongly with the aqueous solvent, which further reduces its tendency to approach and adsorb onto the MMT surface.

3. Crystal Violet and Congo Red Adsorption

In this system, both CV and CR molecules were introduced simultaneously. The total number of dye molecules was set to 20, 30, and 40, and for each total concentration, the CV: CR ratio was varied to evaluate how dye loading and composition influence the ability of MMT to adsorb CV and CR. All mixed dye systems were simulated for 50 ns during the production stage.

Table 3 shows that the highest adsorption was obtained for the system containing 20 molecules with a CV: CR ratio of 3:1. The decline in adsorption capacity observed at higher total dye loadings may indicate that the MMT model, consisting of 84 unit cells (12 × 7 × 1), had approached its maximum adsorption capacity. Among the tested conditions, the mixed system with 20 molecules at a CV: CR ratio of 3:1 yielded the most optimal performance. Therefore, the corresponding trajectory files were further analyzed to investigate the orientations of CV and CR functional groups relative to the MMT surface using RDF profiles, partial density distributions, and diffusion coefficients for CV and CR.

The mixed dye system exhibits interaction behavior that differs from that of the single dye systems. In addition to interactions between the adsorbent and each adsorbate, interactions also occur between different types of adsorbates, which can influence their overall adsorption behavior on the adsorbent. In this study, such interactions lead to an enhanced adsorption of CR onto MMT compared with the single CR system.

.

Table 3. Variations in the addition of CV-CR to each system.

Number of Molecules	CV: CR	Initial Number of CV	Initial Number of CR	Number of CV Adsorbed (VdW)	Number of CR Adsorbed (VdW)
20	1 : 1	10	10	-	-
	3 : 1	15	5	8	2
	3 : 2	12	8	5	2
	4 : 1	16	4	4	1
30	1 : 1	15	15	-	-
	2 : 1	20	10	-	-
	3 : 2	18	12	2	-
	4 : 1	24	6	-	-
40	1 : 1	20	20	4	1
	3 : 1	30	10	3	-
	3 : 2	24	16	-	-
	4 : 1	32	8	1	-

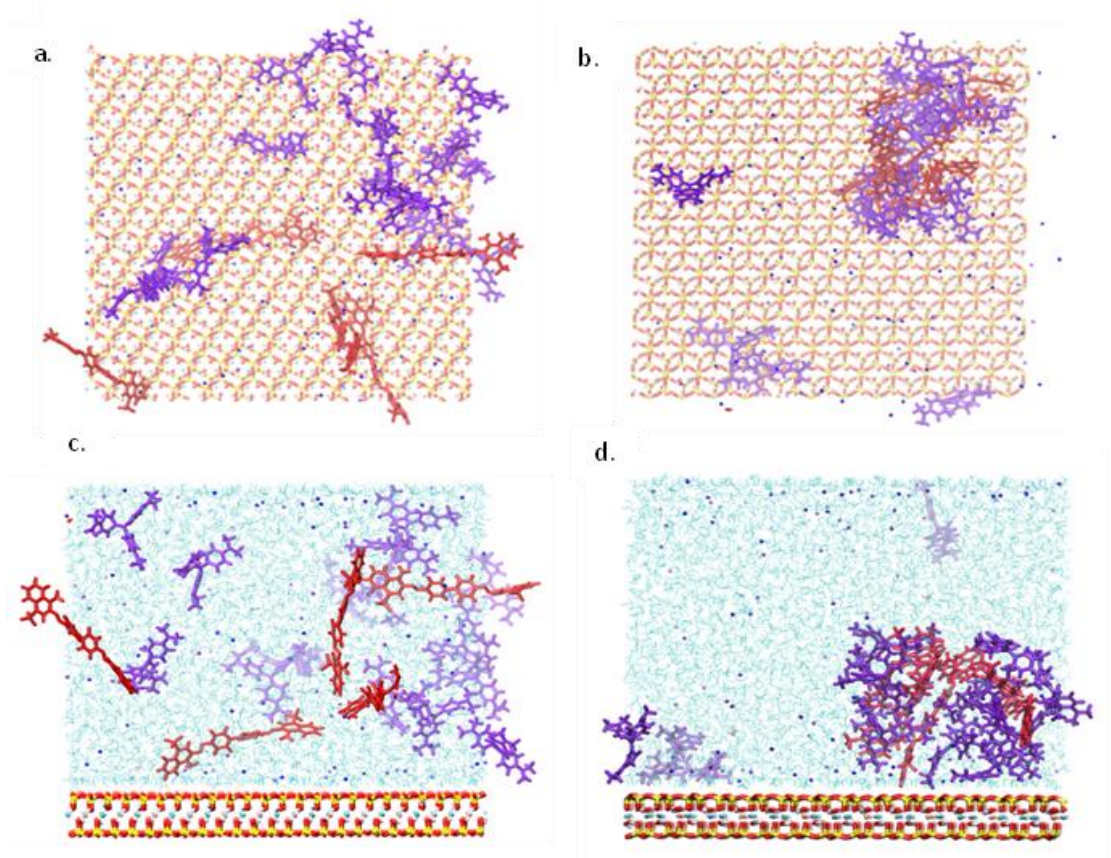

Figure 9. Snapshot of the final results of the 20 CV-CR (3:1) simulation: a. top view before the simulation; b. top view after the simulation; c. front view before the simulation; d. front view after the simulation (Red: CR, Purple: CV)

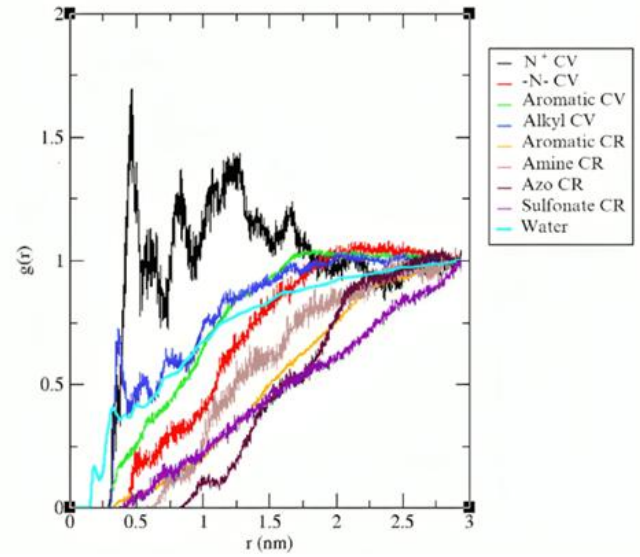

Figure 10. RDF between the functional group of CV-CR and the oxygen atom on the MMT surface.

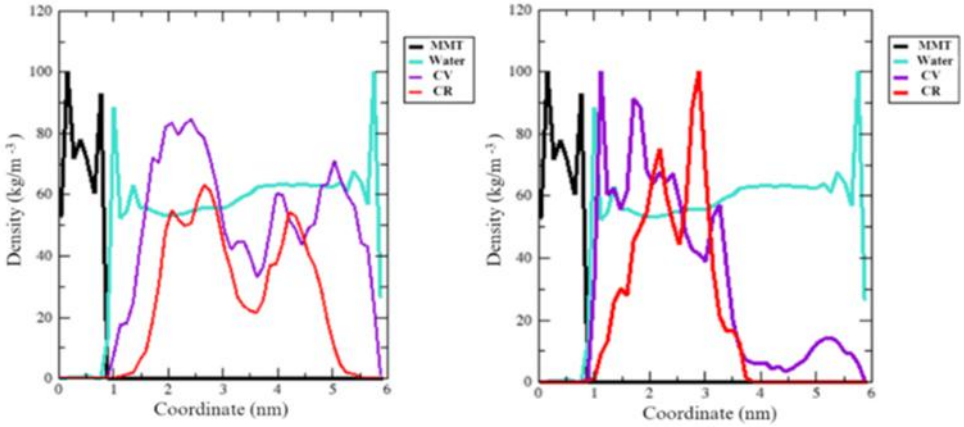

Figure 11. Normalized Partial Density of CV-CR System (20 (3:1)); a. Before production; b. After production

Figure 9 shows that CV and CR molecules were initially dispersed throughout the system before the production run. After 50 ns of simulation, CV and CR molecules interacted with each other, forming aggregates that were subsequently adsorbed onto the MMT surface. The results indicate that CR preferentially interacts with CV, effectively becoming associated with or partially covered by CV molecules. As reported in previous studies [47], textile wastewater typically contains mixtures of different dyes, and interactions among these dyes can either enhance or inhibit their adsorption onto an adsorbent. In a single dye system, MMT does not adsorb CR due to electrostatic repulsion between the negatively charged MMT surface and the anionic CR molecules.

However, the presence of CV in the mixed system, which acts as a cationic dye, can help facilitate the adsorption of CR on the MMT surface. The negatively charged CR interacts with CV to form a complex or aggregate. The MMT surface adsorbs this aggregate through van der Waals interaction.

The RDF profiles in Figure 10 indicate that the dominant functional group interacting with the MMT surface is the N^+ site of CV, consistent with the single CV system. In contrast, the CR functional groups are primarily oriented toward the surrounding water solvent. This suggests competition between CR MMT interactions and the water MMT interactions, with water remaining more strongly associated with the MMT surface than CR.

Interactions among CV, CR, and MMT were further examined using partial density analysis. Partial density describes the density distribution of each species along the simulation coordinates. It can be used to infer the position of a molecule relative to other components in the system [40]. As shown in Figure 11, before the production run, the CV and CR density profiles are broad and located relatively far from the MMT surface, indicating that both dyes are dispersed in the bulk solution. After 50 ns, the CV and CR density peaks become sharper and shift closer to the MMT surface. The sharp peaks indicate aggregation at specific coordinates

and a stronger association with the MMT surface region. The onset of the CR density profile is also lower than that of CV, suggesting that part of CR is effectively covered or shielded by CV during adsorption, which facilitates CR retention near the MMT surface.

This observation is consistent with experimental reports on the coadsorption of cationic and anionic dyes on MMT. Cationic dyes can enter the interlayer space through ion exchange and form an organic-rich phase within the interlayer. Subsequently, anionic dyes may be immobilized within this phase through hydrophobic interactions formed between the adsorbent and the intercalated cationic dye molecules [19].

The relatively weak association of CR with MMT is also reflected in its diffusion coefficient (D). The diffusion coefficient describes molecular mobility in solution and can be estimated from the slope of the MSD curve [40]. As shown in Table 4, CR exhibits a smaller diffusion coefficient than CV. This is likely due to the larger molecular size and higher molecular mass of CR, which reduces its mobility relative to CV. Additionally, the stronger hydrogen bonding between CR and water in the single dye system (Figure 8) can further decrease CR mobility, contributing to its lower diffusion coefficient. In the mixed dye system, the diffusion coefficients of both CV and CR decrease. This reduction can be attributed to strong dye-dye interactions between CV and CR, including electrostatic attractions, which promote aggregation and limit overall molecular mobility.

Table 4. Diffusion coefficient (D) values of CV and CR in single and mixed systems

System	D (10^{-5} cm^2/s)
CV (single)	0,1125
CV (mixed)	0,0708
CR (single)	0,0641
CR (mixed)	0,0193

CONCLUSION

Molecular dynamics studies can be used to investigate the adsorption mechanism of cationic and anionic dye mixtures on montmorillonite at the molecular level, and to establish the direct correlation between microscopic details and macroscopic properties of the systems used in the experimental study. This study has investigated the orientation mechanism of CV and CR adsorption on MMT, both in single and mixed systems. In the single CV system, the optimal adsorption capacity is achieved when 20 CVs are added, resulting in an adsorption percentage of 40%. CV is adsorbed on the surface of MMT through a dominant van der Waals interaction occurring between the surface of MMT and the quaternary amine group ($–N^+$) on the CV molecule. In the single CR system, no CR molecules are adsorbed due to the

electrostatic repulsive force between the CR and MMT surfaces. In the mixed system, there is an increase in the adsorption capacity of CV and CR. The system that yields optimal results is one in which the number of CV-CR is increased by 20 molecules, with a CV: CR ratio of 3:1. This system exhibits a synergistic interaction between CV and CR, enabling an increase in adsorption capacity to 50%.

REFERENCES

[1] F. Norman, "Key Factors to Promote Industry 4.0 Readiness at Indonesian Textile and Clothing Firm," *Engineering, Mathematics and Computer Science (EMACS) Journal*, vol. 2, no. 2, pp. 73–83, 2020, doi: 10.21512/emacsjournal.v2i2.6448.

[2] M. M. Mubyarto and G. P. D. Sohibien, "Determinants of Competitiveness of the Leading Manufacturing Sector for Making Indonesia 4.0 Program," Seminar Nasional Official Statistics, pp. 710–719, 2019, doi: 10.34123/semnasoffstat.v2019i1.56.

[3] "G. A. F. A. Adjid, A. Kurniawan, and Nazriati, "Textile Industry Waste Pollution in the Konto River: A Comparison of Public Perceptions and Water Quality Data," *J. Exp. Life Sci.*, vol. 12, no. 3, 2022, doi: 10.21776/ub.jels.2022.012.03.05

[4] J. C. Wara Angi, N. H. Al Mukarramah, and M. Maskun, "Mitigating water depletion through wastewater management law in Indonesia's textile sector: Evaluating compliance and alignment with national environmental standards," in BIO Web of Conferences, EDP Sciences, Jan. 2025. doi: 10.1051/bioconf/202515506017.

[5] U. T. Gomes *et al*., "Dye Schedule Optimization: A Case Study in a Textile Industry," *Applied Sciences*, vol. 11, no. 14, Art. no. 6467, 2021, doi: 10.3390/app11146467.

[6] I. A. Aguayo-Villarreal, D. Cortes-Arriagada, C. K. Rojas-Mayorga, K. Pineda-Urbina, R. Muñiz-Valencia, and J. González, "Importance of the interaction adsorbent –adsorbate in the dyes adsorption process and DFT modeling," J Mol Struct, vol. 1203, Mar. 2020, doi: 10.1016/j.molstruc.2019.127398.

[7] S. Benabid, A. F. M. Streit, Y. Benguerba, G. L. Dotto, A. Erto, and B. Ernst, "Molecular modeling of anionic and cationic dyes adsorption on sludge-derived activated carbon," J Mol Liq, vol. 289, p. 111119, Sep. 2019, doi: 10.1016/j.molliq.2019.111119.

[8] E. J. Weber and V. C. Stickney, "Hydrolysis Kinetics of Reactive Blue 19-Vinyl Sulfone," War. Res, vol. 27, no. 1, pp. 63–67, 1993. 10.1016/0043-1354(93)90195-N.

[9] S. Dutta, B. Gupta, S. K. Srivastava, and A. K. Gupta, "Recent advances on the removal of dyes from wastewater using various adsorbents: A critical review," Jul. 21, 2021, Royal Society of Chemistry. doi: 10.1039/d1ma00354b.

[10] Y. Tian et al., "Biodegradation and Decolorization of Crystal Violet Dye by Cocultivation with Fungi and Bacteria," ACS Omega, 2023, doi: 10.1021/acsomega.3c06978.

[11] A. A. A. Kamal et al., "Electrocoagulation for dye removal in wastewater: A preliminary study using full factorial design," in Journal of Physics: Conference Series, Institute of Physics, 2025. doi: 10.1088/1742-6596/3003/1/012033.

[12] A. E. Abdelhamid, A. E. Elsayed, M. Naguib, and E. A. B. Ali, "Effective Dye Removal by Acrylic-Based Membrane Constructed from Textile Fibers Waste," Fibers and Polymers, vol. 24, no. 7, pp. 2391–2399, Jul. 2023, doi: 10.1007/s12221-023-00247-z.

[13] M. M. Naim, N. F. Al-Harby, M. El Batouti, and M. M. Elewa, "Macro-Reticular Ion Exchange Resins for Recovery of Direct Dyes from Spent Dyeing and Soaping Liquors," Molecules, vol. 27, no. 5, Mar. 2022, doi: 10.3390/molecules27051593.

[14] A. Benalia, K. Derbal, O. Baatache, C. Lehchili, A. Khalfaoui, and A. Pizzi, "Removal of Dyes from Water Using Aluminum-Based Water Treatment Sludge as a Low-Cost Coagulant: Use of Response Surface Methodology," Water (Switzerland), vol. 16, no. 10, May 2024, doi: 10.3390/w16101400.

[15] D. A. Bopape, B. Ntsendwana, and F. D. Mabasa, "Photocatalysis as a pre-discharge treatment to improve the effect of textile dyes on human health: A critical review," Oct. 30, 2024, Elsevier Ltd. doi: 10.1016/j.heliyon.2024.e39316.

[16] A. Imessaoudene et al., "Adsorption Performance of Zeolite for the Removal of Congo Red Dye: Factorial Design Experiments, Kinetic, and Equilibrium Studies," Separations, vol. 10, no. 1, Jan. 2023, doi: 10.3390/separations10010057.

[17] S. Kato and Y. Kansha, "Comprehensive review of industrial wastewater treatment techniques," Aug. 01, 2024, Springer. doi: 10.1007/s11356-024-34584-0.

[18] R. El Haouti et al., "Cationic dyes adsorption by Na-Montmorillonite Nano Clay: Experimental study combined with a theoretical investigation using DFT-based descriptors and molecular dynamics simulations," J Mol Liq, vol. 290, Sep. 2019, doi: 10.1016/j.molliq.2019.111139.

[19] Q. Zhang et al., "Adsorption of cationic and anionic dyes on montmorillonite in single and mixed wastewater," Journal of Porous Materials, vol. 26, no. 6, pp. 1861–1867, Dec. 2019, doi: 10.1007/s10934-019-00782-2.

[20] H. Ouachtak et al., "Highly efficient and fast batch adsorption of orange G dye from polluted water using superb organo-montmorillonite: Experimental study and molecular dynamics investigation," J Mol Liq, vol. 335, Aug. 2021, doi: 10.1016/j.molliq.2021.116560.

[21] K. Z. Elwakeel, A. M. Elgarahy, G. A. Elshoubaky, and S. H. Mohammad, "Microwave assist sorption of crystal violet and Congo red dyes onto amphoteric sorbent based on upcycled Sepia shells 03 Chemical Sciences 0306 Physical Chemistry (incl. Structural)," J Environ Health Sci Eng, vol. 18, no. 1, pp. 35–50, Jan. 2020, doi: 10.1007/s40201-019-00435-1.

[22] K. M. Doke, M. Yusufi, R. D. Joseph, and E. M. Khan, "Comparative Adsorption of Crystal Violet and Congo Red onto ZnCl2 Activated Carbon," J Dispers Sci Technol, vol. 37, no. 11, pp. 1671–1681, Nov. 2016, doi: 10.1080/01932691.2015.1124342.

[23] S. Bentahar, A. Dbik, M. El Khomri, N. El Messaoudi, and A. Lacherai, "Adsorption of methylene blue, crystal violet and congo red from binary and ternary systems with natural clay: Kinetic, isotherm, and thermodynamic," J Environ Chem Eng, vol. 5, no. 6, pp. 5921–5932, Dec. 2017, doi: 10.1016/j.jece.2017.11.003.

[24] Çoruh S, Elevli S, and Doğan G, "Optimization study of adsorption of

crystal violet and congo red onto sepiolite and clinoptilolite," Global NEST Journal, vol. 19, no. 2, pp. 336–343, 2017, doi: 10.30955/gnj.002128.

[25] C. M. Oloo, J. M. Onyari, W. C. Wanyonyi, J. N. Wabomba, and V. M. Muinde, "Adsorptive removal of hazardous crystal violet dye form aqueous solution using Rhizophora mucronata stem-barks: Equilibrium and kinetics studies," Environmental Chemistry and Ecotoxicology, vol. 2, pp. 64–72, Jan. 2020, doi: 10.1016/j.enceco.2020.05.001.

[26] S. Thakur, S. Singh, and B. Pal, "Superior adsorptive removal of brilliant green and phenol red dyes mixture by CaO nanoparticles extracted from egg shells," J Nanostructure Chem, vol. 12, no. 2, pp. 207–221, Apr. 2022, doi: 10.1007/s40097-021-00412-x.

[27] L. Liu et al., "Simultaneous removal of cationic and anionic dyes from environmental water using montmorillonite-pillared graphene oxide," J Chem Eng Data, vol. 60, no. 5, pp. 1270–1278, May 2015, doi: 10.1021/je5009312.

[28] N. Hamad, A. A. Galhoum, A. Saad, and S. Wageh, "Efficient adsorption of cationic and anionic dyes using hydrochar nanoparticles prepared from orange peel," J Mol Liq, vol. 409, Sep. 2024, doi: 10.1016/j.molliq.2024.125349.

[29] R. El Haouti et al., "Cationic dyes adsorption by Na-Montmorillonite Nano Clay: Experimental study combined with a theoretical investigation using DFT-based descriptors and molecular dynamics simulations," J Mol Liq, vol. 290, p. 111139, Sep. 2019, doi: 10.1016/j.molliq.2019.111139.

[30] H. Ouachtak et al., "Experimental and molecular dynamics simulation study on the adsorption of Rhodamine B dye on magnetic montmorillonite composite γ-Fe2O3@Mt," J Mol Liq, vol. 309, Jul. 2020, doi: 10.1016/j.molliq.2020.113142.

[31] M. Zhang, H. Mao, and Z. Jin, "Molecular dynamic study on structural and dynamic properties of water, counter-ions and polyethylene glycols in Na-montmorillonite interlayers," Appl Surf Sci, vol. 536, Jan. 2021, doi: 10.1016/j.apsusc.2020.147700.

[32] O. S. Omer, B. H. M. Hussein, A. M. Ouf, M. A. Hussein, and A. Mgaidi, "An organified mixture of illite-kaolinite for the removal of Congo red from wastewater," Journal of Taibah University for Science, vol. 12, no. 6, pp. 858–866, 2018, doi: 10.1080/16583655.2018.1540179.

[33] M. Said, L. Indwi Saputri, Hasanudin, P. Loekitowati Hariani, and N. L. Yong, "Kinetic Study of Removal of Congo Red and Direct Green," in IOP Conference Series: Earth and Environmental Science, IOP Publishing Ltd, Aug. 2021. doi: 10.1088/1755-1315/810/1/012048.

[34] M. M. F. Silva, M. M. Oliveira, M. C. Avelino, M. G. Fonseca, R. K. S. Almeida, and E. C. Silva Filho, "Adsorption of an industrial anionic dye by modified-KSF-montmorillonite: Evaluation of the kinetic, thermodynamic and equilibrium data," Chemical Engineering Journal, vol. 203, pp. 259–268, Sep. 2012, doi: 10.1016/j.cej.2012.07.009.

[35] A. Lindahl, Hess, and van der Spoel, "GROMACS 2021.4 Manual (2021.4)," 2021, Zenodo. doi: 10.5281/zenodo.5636522.

[36] S. Jo, T. Kim, V. G. Iyer, and W. Im, "CHARMM-GUI: A web-based

graphical user interface for CHARMM," J Comput Chem, vol. 29, no. 11, pp. 1859–1865, Aug. 2008, doi: 10.1002/jcc.20945.

[37] S. Tesson, M. Salanne, B. Rotenberg, S. Tazi, and V. Marry, "A Classical Polarizable Force Field for Clays: Pyrophyllite and Talc," Journal of Physical Chemistry C, vol. 120, no. 7, 2016, doi: 10.1021/acs.jpcc.5b10181ï.

[38] J. Lee et al., "CHARMM-GUI Input Generator for NAMD, GROMACS, AMBER, OpenMM, and CHARMM/OpenMM Simulations Using the CHARMM36 Additive Force Field," J Chem Theory Comput, vol. 12, no. 1, pp. 405–413, Jan. 2016, doi: 10.1021/acs.jctc.5b00935.

[39] X. Wu et al., "Molecular dynamics simulation of the interaction between common metal ions and humic acids," Water (Switzerland), vol. 12, no. 11, pp. 1–11, Nov. 2020, doi: 10.3390/w12113200.

[40] F. Largo et al., "Adsorptive removal of both cationic and anionic dyes by using sepiolite clay mineral as adsorbent: Experimental and molecular dynamic simulation studies," J Mol Liq, vol. 318, Nov. 2020, doi: 10.1016/j.molliq.2020.114247.

[41] W. Wu et al., "Study of the aggregation behaviour of three primary reactive dyes via molecular dynamics simulations," Mol Simul, vol. 46, no. 8, pp. 627–637, May 2020, doi: 10.1080/08927022.2020.1755037.

[42] F. Castillo-Borja and U. I. Bravo-Sánchez, "Aluminum adsorption using different models of hydroxyapatite via Molecular Dynamic simulations," J Mol Liq, vol. 395, Feb. 2024, doi: 10.1016/j.molliq.2023.123899.

[43] A. Kühnle, "Self-assembly of organic molecules at metal surfaces," Curr Opin Colloid Interface Sci, vol. 14, no. 2, pp. 157–168, Apr. 2009, doi: 10.1016/j.cocis.2008.01.001.

[44] J. L. Marco-Brown et al., "New insights on crystal violet dye adsorption on montmorillonite: Kinetics and surface complexes studies," Chemical Engineering Journal, vol. 333, pp. 495–504, Feb. 2018, doi: 10.1016/j.cej.2017.09.172.

[45] Z. Li et al., "Solid-liquid equilibrium behavior and thermodynamic analysis of p-aminobenzoic acid using experimental measurement and molecular dynamic simulation," J Mol Liq, vol. 323, Feb. 2021, doi: 10.1016/j.molliq.2020.114964.

[46] J. Chanra, E. Budianto, and B. Soegijono, "Surface modification of montmorillonite by the use of organic cations via conventional ion exchange method," in IOP Conference Series: Materials Science and Engineering, Institute of Physics Publishing, May 2019. doi: 10.1088/1757-899X/509/1/012057.

[47] K. Sharma, A. K. Dalai, and R. K. Vyas, "Removal of synthetic dyes from multicomponent industrial wastewaters," Reviews in Chemical Engineering, vol. 34, no. 1, pp. 107–134, Dec. 2017, doi: 10.1515/revce-2016-0042.